PROCEEDINGS OF SCIENCE

Recent progress on heavy hadron spectroscopy in LHCb

Youhua Yang[a,*]

[a] *On behalf of LHCb Collaboration*
INFN e University of Genova,
Via Dodecaneso, 33, 16146 Genova GE, Italy

E-mail: youhua.yang@cern.ch

Spectroscopy of heavy hadrons offers a powerful tool for exploring the intricacies of Quantum Chromodynamics. In hadron spectroscopy, experimental studies, in particular the discovery of new hadronic states, are essential for understanding the nature of exotic hadrons. The extensive flavor dataset collected by the LHCb experiment during the LHC operating periods 2011-2012 and 2015-2018 presents a unique opportunity to investigate the internal structure of hadrons and deepen our understanding of strong interactions. This talk will highlight the latest advancements in hadron spectroscopy, leveraging insights gained from these comprehensive datasets.

The 43rd International Symposium on Physics in Collision (PIC2024)
22-25 Oct, 2024
National Centre for Scientific Research "Demokritos", Athens, Greece

*Speaker

© Copyright owned by the author(s) under the terms of the Creative Commons Attribution-NonCommercial-NoDerivatives 4.0 International License (CC BY-NC-ND 4.0) All rights for text and data mining, AI training, and similar technologies for commercial purposes, are reserved. ISSN 1824-8039 . Published by SISSA Medialab.

PoS(PIC2024)059

PROCEEDINGS OF SCIENCE

1. Introduction

In heavy quark spectroscopy, the focus is on the mass spectrum and properties of hadrons containing heavy quarks like charm and beauty. Hadrons, composed of quarks bound by gluons, are described by Quantum Chromodynamics (QCD), which works well at high energies but struggles at low energies, making first-principle descriptions difficult. Experimental studies, combined with lattice QCD and phenomenological models, are crucial for advancing our understanding of non-perturbative QCD and hadronic dynamics.

Besides conventional hadrons (mesons and baryons), the discovery of exotic hadrons offers further insight into hadronic structure. Exotic hadrons are believed to consist of more complex quark configurations. Numerous theoretical models have been proposed to explain these exotic states, which can be broadly categorized into two main groups: compact multiquark states and molecular states. These proceedings report recent progress on both conventional and exotic hadrons from LHCb, contributing significantly to the understanding of hadronic dynamics.

2. Exotic states studies

2.1 Tetraquark states

2.1.1 Probing the nature of the $\chi_{c1}(3872)$ state using radiative decays

The first charmonium-like state $\chi_{c1}(3872)$, which is not associated with any conventional charmonium resonance, was observed more than two decades ago. Its quantum number is 1^{++} but its internal structure remains unclear. The LHCb collaboration reported the first evidence for the decay $B^+ \to \chi_{c1}(3872)K^+$, where $\chi_{c1}(3872) \to \psi(2S)\gamma$, by measuring the ratio of the branching fraction

$$\mathcal{R} = \frac{\mathcal{B}_{B^+\to(\chi_{c1}(3872)\to\psi(2S)\gamma)K^+}}{\mathcal{B}_{B^+\to(\chi_{c1}(3872)\to J/\psi\gamma)K^+}} = 1.67 \pm 0.21 \pm 0.12 \pm 0.04. \quad (1)$$

Given that the mass of $X_{c1}(3872)$ is very close to the $D^0\bar{D}^{0*}$ threshold,it is often described within the molecular model. However, the molecular interpretation conflicts with results suggesting a high production cross-section, which is more consistent with conventional charmonium states. Moreover, several other hypotheses have been proposed, including the mixing of molecular and charmonium states and the virtual companion pole model.

LHCb has observed the radiative decay [1] for both RUN I and RUN II data as shown in Fig. 1. The measured results do not support the molecular model, though more statistics are needed to fully understand the nature of $\chi_{c1}(3872)$.

2.2 Search for charmonium(-like) state in $B^+ \to DDh$ decays

The LHCb collaboration has initiated a category of $B^+ \to D\overline{D}h$ decays, where h is meson, starting with an amplitude analysis of $B^+ \to D^+D^-K^+$ [2, 3], where conventional resonances can only contribute to the D^+D^- system. This provides a clean environment for studying charmonium-like states. A spin-2 particle, $\chi_{c2}(3930)$, has been observed, as predicted. Furthermore, this analysis made of the first observation of open-charm tetraquark candidates, $T_{cs0/1}(2900)$, and sparked a series of searches of such states.

Subsequently, the $B^+ \to D_s^+D_s^-K^+$ decay [4] revealed the charmonium-like state $X(3920)$. Two manifested T_{cs} states, namely the doubly charged $T_{c\bar{s}}(2900)^{++}$ and $T_{c\bar{s}0}(2900)^0$, were observed in the decays $B^0 \to \overline{D}^0D_s^+\pi^-$ and $B^+ \to D^-D_s^+\pi^-$ [5, 6], respectively.

© Copyright owned by the author(s) under the terms of the Creative Commons
Attribution-NonCommercial-NoDerivatives 4.0 International License (CC BY-NC-ND 4.0).

PoS(PIC2024)059

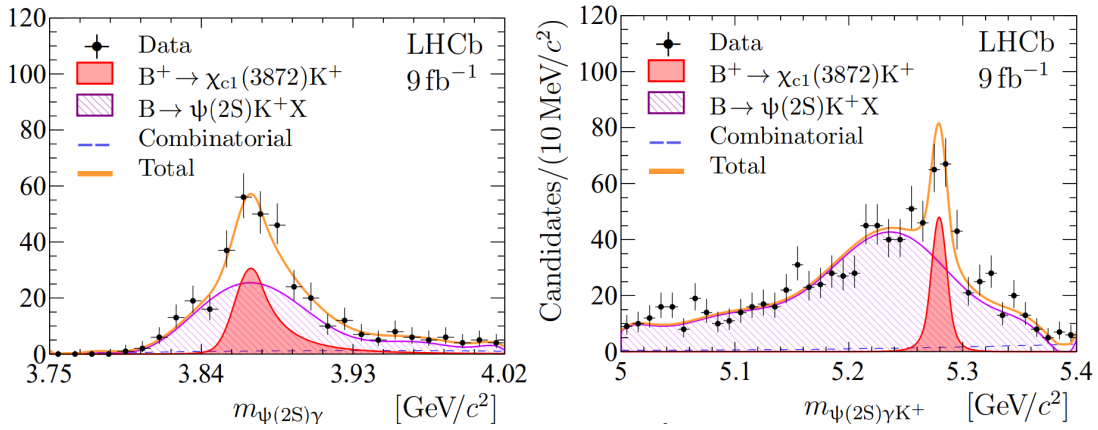

Figure 1: Distributions of the (right) $\psi\gamma K^+$ and (left) $\psi\gamma$ mass of selected B candidates summed over RUN 1 and Run 2 data-taking periods.

To validate the T_{cs} state and search for new charmonium-like states, an amplitude analysis was performed in decays $B^+ \to D^{*+}D^-K^+$ and $B^+ \to D^{*-}D^+K^+$ simultaneously. The links between the $D^{*+}D^-$ and $D^{*-}D^+$ systems enables the measurement of the C-parity. This feature was utilised in an amplitude analysis for the first time.

Four resonances, $\eta_c(3945)$, $h_c(4000)$, $\chi_{c1}(4010)$, and $h_c(4300)$, have been observed in the $D^{*\pm}D^{\mp}$ system, as seen in Fig. 2, where the latter three resonances were observed for the first time [7]. The quantum numbers J^{PC} for these four resonances were determined to be 0^{-+}, 1^{+-}, 1^{++}, and 1^{+-}, respectively.

The spin-0 and spin-1 T_{cs} states were observed in the $D^{*-}K^+$ system, confirming previous findings in the amplitude analysis of $B^+ \to D^-D^+K^+$. However, tension with a 2σ significance as shown in table 1 in the branching fraction for the T_{cs0} indicates that the production mechanism of the T_{cs} state requires further investigation.

Table 1: Comparison of the $T^{*0}_{\bar{c}\bar{s}0,1}$ properties obtained in Ref. [7] to those found previously in $B^+ \to D^+D^-K^+$ decays [2, 3]. In the measurement branching fractions, the $T^{*0}_{\bar{c}\bar{s}0,1}$ masses and widths are fixed to the previously measured values [2, 3].

Property	$B^+ \to D^{*\pm}D^{\mp}K^+$ [7]	$B^+ \to D^+D^-K^+$ [2, 3]
$T^*_{\bar{c}\bar{s}0}(2870)^0$ mass [MeV]	$2914 \pm 11 \pm 15$	2866 ± 7
$T^*_{\bar{c}\bar{s}0}(2870)^0$ width [MeV]	$128 \pm 22 \pm 23$	57 ± 13
$T^*_{\bar{c}\bar{s}1}(2900)^0$ mass [MeV]	$2887 \pm 8 \pm 6$	2904 ± 5
$T^*_{\bar{c}\bar{s}1}(2900)^0$ width [MeV]	$92 \pm 16 \pm 16$	110 ± 12
$\mathcal{B}(B^+ \to T^*_{\bar{c}\bar{s}0}(2870)^0 D^{(*)+})$	$(4.5\,^{+0.6}_{-0.8}\,^{+0.9}_{-1.0} \pm 0.4) \times 10^{-5}$	$(1.2 \pm 0.5) \times 10^{-5}$
$\mathcal{B}(B^+ \to T^*_{\bar{c}\bar{s}1}(2900)^0 D^{(*)+})$	$(3.8\,^{+0.7}_{-1.0}\,^{+1.6}_{-1.1} \pm 0.3) \times 10^{-5}$	$(6.7 \pm 2.3) \times 10^{-5}$
$\frac{\mathcal{B}(B^+ \to T^*_{\bar{c}\bar{s}0}(2870)^0 D^{(*)+})}{\mathcal{B}(B^+ \to T^*_{\bar{c}\bar{s}1}(2900)^0 D^{(*)+})}$	$1.17 \pm 0.31 \pm 0.48$	0.18 ± 0.05

Previous results on the $D_s^+\pi^\pm$ system found the doubly charged tetraquark $T_{c\bar{s}0}(2900)^{++}$ and its neutral partner $T_{c\bar{s}0}(2900)^0$. To search for new charmonium-like and $T_{c\bar{s}}$ states and to confirm the observed doubly charged $T_{c\bar{s}0}(2900)^{++}$, LHCb performed another study of $B \to D\overline{D}h$ decays, focusing on the charm-strange meson system $B^+ \to D^{*-}D_s^{(*)+}\pi^+$, using the full RUN I and RUN II datasets [8]. The relative branching

PoS(PIC2024)059

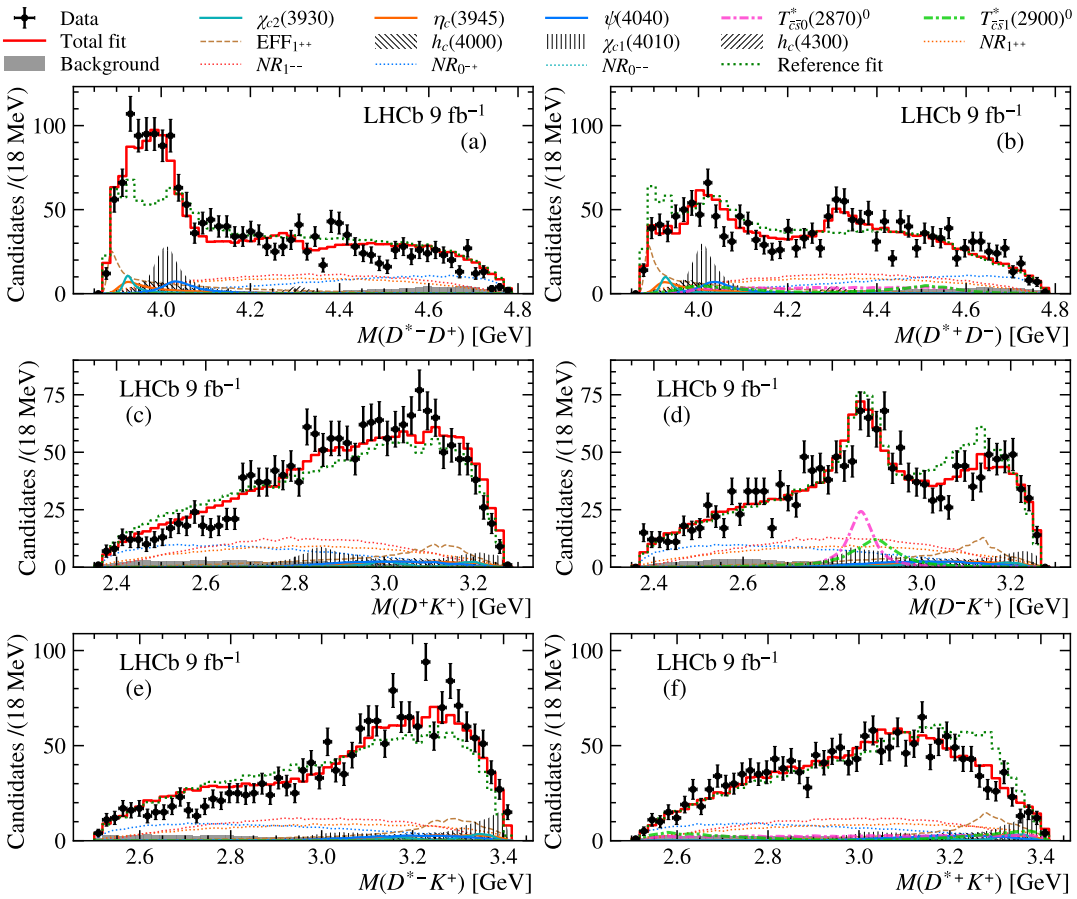

Figure 2: Distributions of two-body invariant masses: (a) $M(D^{*-}D^+)$, (c) $M(D^+K^+)$ and (e) $M(D^{*-}K^+)$ in the $B^+ \to D^{*-}D^+K^+$, (c) $M(D^+D^-)$, $M(D^-K^+)$ and (e) $M(D^{*+}K^+)$ in the $B^+ \to D^{*+}D^-K^+$ sample.

fractions for the decays $B^+ \to D^{*-}D_s^+\pi^+$ and $B^+ \to D^{*-}D_s^{*+}\pi^+$ are determined to be:

$$\frac{\mathcal{B}(B^+ \to D^{*-}D_s^+\pi^+)}{\mathcal{B}(B^0 \to D^{*-}D_s^+)} = 0.173 \pm 0.006 \pm 0.010,$$
$$\frac{\mathcal{B}(B^+ \to D^{*-}D_s^{*+}\pi^+)}{\mathcal{B}(B^0 \to D^{*-}D_s^+\pi^+)} = 1.32 \pm 0.07 \pm 0.14,$$

where the first uncertainty is statistical and the second systematic.

An amplitude analysis of $B^+ \to D^{*-}D_s^+\pi^+$ decay was performed, using a sample defined in the range of the nominal B^+ mass ± 30 MeV/c^2. In the baseline model, only resonances in the $D^{*-}\pi^+$ system were considered. Figure 3 presents observations of the $D_0(2550)$ and $D_1^*(2600)$ resonances in the best fit, with significance values of 6.5σ and 6.8σ, respectively.

In the newly produced amplitude analysis $B^- \to D^-D^0K_S^0$ decays [9], spin-0 T_{cs}^0 is observed with significance 5.3σ, while no significant signal found for spin-1 T_{cs}^0.

The properties of spin-0 $T_{c\bar{s}0}$ are consistent with $B^+ \to D^{*\pm}D^{\mp}K^+$. The isospin symmetry requires the relative widths between the $T_{cs}^{*0} \to D^0K_S^0$ and $T_{cs}^{*0} \to D^+K^-$ decays to be $R_I(T_{cs}^{*0}) \equiv \Gamma(T_{cs}^{*0} \to D^0\bar{K}^0)/\Gamma(T_{cs}^{*0} \to D^+K^-) \approx 1$. In addition, $R_{FF}(D^0K_S^0/D^+K^-) \equiv R_{FF}(D^0K_S^0)/R_{FF}(D^+K^-)$ are expected to be 1, where $R_{FF}(D^0K_S^0) = FF(T_{cs1}^{*0} \to D^0K_S^0)/FF(T_{cs0}^{*0} \to D^0K_S^0)$, is the ratio between spin-1 and

PoS(PIC2024)059

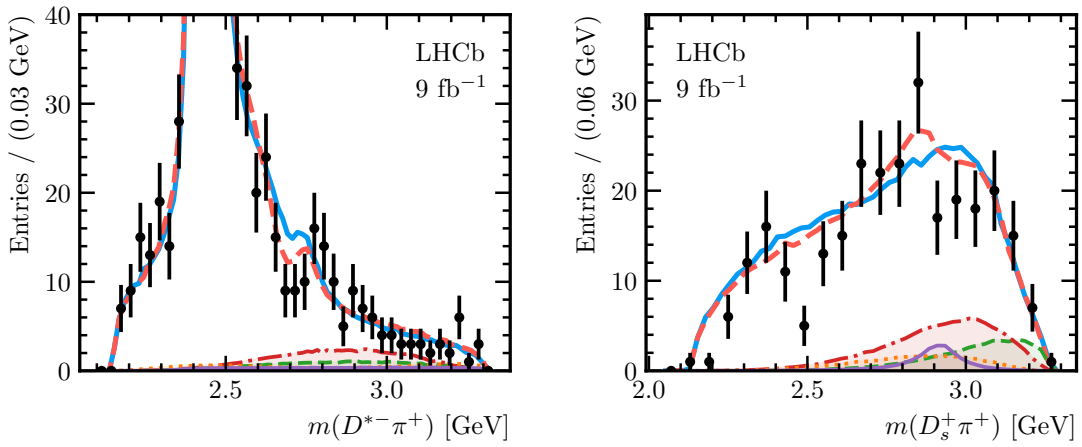

Figure 3: Comparison of the fit results of the $B \to D^{*-}D_s^+\pi^+$ distribution with the baseline model and with the model that includes $D_s^+\pi^+$ components. The $m(D^{*-}\pi^+)$ and $m(D_s^+\pi^+)$ are shown in left and right respectively.

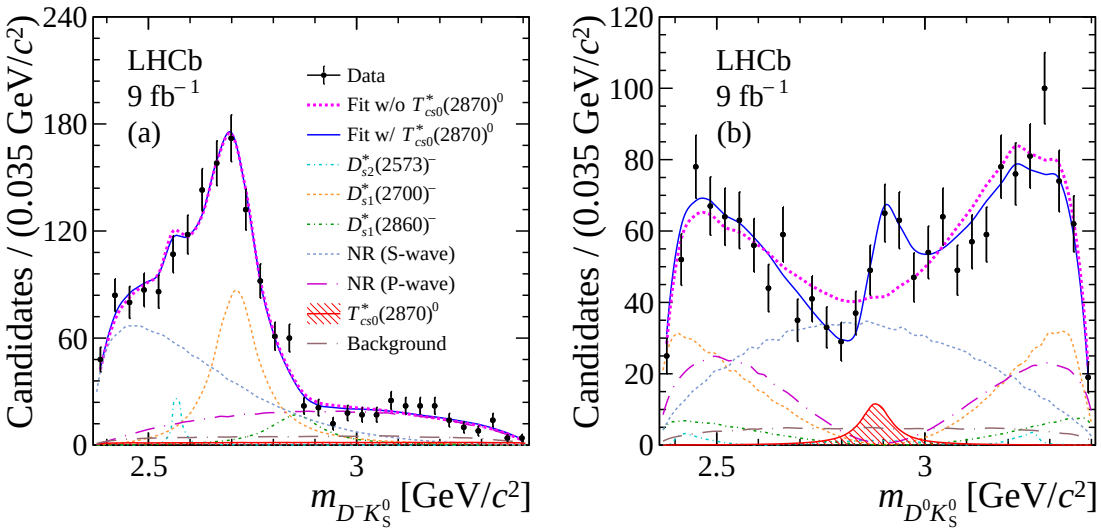

Figure 4: Mass distributions of (a) $m(D^0K^0_S)$ and (b) $m(D^-K^0_S)$ together with the fit projections with (thick blue) or without (dashed magenta) the $T_{cs}(2870)^0$state.

spin-0 T^*_{cs} state:

$$R_I(T^*_{cs0}(2870)^0) = 3.3 \pm 1.1 \pm 1.1 \pm 1.1,$$
$$R_I(T^*_{cs1}(2870)^0) = 0.15 \pm 0.15 \pm 0.05 \pm 0.05,$$
$$R_{FF}(D^0K^0_S/D^+K^-) = 0.044 \pm 0.035 \pm 0.020,$$

where the first, second and third uncertainties are statistical, systematic and due to the external inputs of $B^- \to D^-D^+K^-$ and $B^- \to D^-D^0K^0_S$ branching fractions, respectively. The measured results show large deviation from unity, which indicate triangle singularity contribution and can not exclude a violation of isospin invariance for spin-1 T_{cs} state if assuming it is genuine hadron.

PoS(PIC2024)059

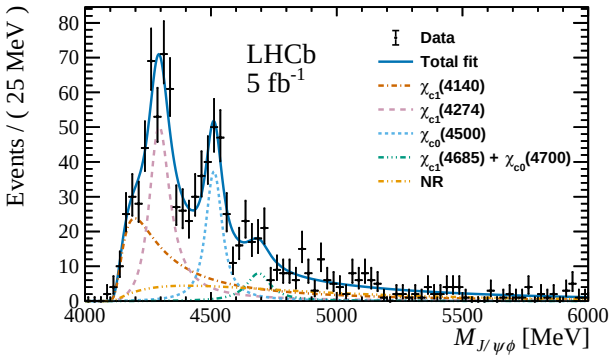

Figure 5: Invariant-mass distribution of $J/\psi(\to \mu^+\mu^-)\phi(K^+K^-)$ candidates in the signal sample after selection. The fit components are shown as dashed lines.

2.3 New production on central exclusive production process

The production of complex states, such as vector-meson pairs, in central diffractive collisions with large rapidity gaps is not well understood, and photon-induced or pomeron-induced processes may offer insights into non-perturbative QCD. The central exclusive production process is particularly clean at the LHC because the colliding protons remain intact, which narrows down the possible spin-parity options of the produced complex states. However, the production rate is relatively low.

LHCb observed several charmonium-like states in the $J/\psi\phi$ system in the diffractive process [10]. In this study, five resonances and one non-resonant component were used to describe the invariant-mass distribution of the $J/\psi\phi$ system very well. The $X_{c1}(4500)$ resonance was observed, as shown in Fig. 5. Overall, this study contributes to a better understanding of the underlying nature of these exotic candidates.

2.4 Pentaquark states

2.4.1 Search for prompt production of pentaquarks in charm hadron final states

Studies of pentaquark states make some progress recently in LHCb. Inspired by the $\Lambda_b^0 \to J/\psi p K^-$ [11], the proximity of $\Sigma_c^+\overline{D}^0$ and $\Sigma_c^+\bar{D}^{*0}$ thresholds to the signal peaks in the open charm region of M($J/\psi p$) suggests threshold effects play an important role in the formation of exotic states. For the compact multiquarks, the mass proximity to the threshold is accidental, molecular states is more likely for the pentaquark.

A search for pentaquark via open-charm final states is performed [12]. Different charm hadrons i.e. Λ_c^+, D^-, D^0, $\Sigma_c^{++/0}$ and D^{*-} are used. The combinations are divided into hidden charm and doubly-charm pentaquarks. However, the results show that no significant signals are found and the upper limits on the fraction $R(\Lambda_c^+)$ are determined,

$$\mathcal{R}(\Lambda_c^+) = \frac{N_P}{N_{\Lambda_c^+}} \times \frac{\epsilon_{\Lambda_c^+}}{\epsilon_P}, \tag{2}$$

where N represents the Λ_c^+ or pentaquark (P) yield and ϵ is the combined trigger and selection efficiency.

2.4.2 First observation of $\Lambda_b^0 \to \Sigma_c^{(*)++} D^{(*)-} K^-$ decays and $\Lambda_b^0 \to \Lambda_c^+ \overline{D}^{(*)0} K^-$ decays

The proximity of pentaquark candidates to the open-charm mass threshold also motivated the study of $\Lambda_b^0 \to \Sigma_c^{(*)++} D^{(*)-} K^-$ for the first time [13]. The molecular pentaquark model predicts a P_ψ^N state with

PoS(PIC2024)059

$\frac{3}{2}^+$ spin-parity, decaying to $\Sigma_c^{(*)++}\bar{D}$. These four Lb decays are observed with high significance, with their relative branching fractions measured to be:

$$\frac{\mathcal{B}(\Lambda_b^0 \to \Sigma_c^{++} D^- K^-)}{\mathcal{B}(\Lambda_b^0 \to \Lambda_c^+ \overline{D}^0 K^-)} = 0.282 \pm 0.016 \pm 0.016 \pm 0.005,$$
$$\frac{\mathcal{B}(\Lambda_b^0 \to \Sigma_c^{*++} D^- K^-)}{\mathcal{B}(\Lambda_b^0 \to \Sigma_c^{++} D^- K^-)} = 0.460 \pm 0.052 \pm 0.028,$$
$$\frac{\mathcal{B}(\Lambda_b^0 \to \Sigma_c^{++} D^{*-} K^-)}{\mathcal{B}(\Lambda_b^0 \to \Sigma_c^{++} D^- K^-)} = 2.261 \pm 0.202 \pm 0.129 \pm 0.046,$$
$$\frac{\mathcal{B}(\Lambda_b^0 \to \Sigma_c^{*++} D^{*-} K^-)}{\mathcal{B}(\Lambda_b^0 \to \Sigma_c^{++} D^- K^-)} = 0.896 \pm 0.137 \pm 0.066 \pm 0.018,$$

where the first uncertainties are statistical, the second systematic, and the third are due to uncertainties on the branching fractions of intermediate particle decays. Large statistics of these channels is collected in these analysis, which paves the way for amplitude analysis in the upcoming Run 3 data with higher efficiency and higher luminosity.

Similarly, another promising search was performed for the first time in the channel $\Lambda_b^0 \to \Lambda_c^+ \overline{D}^{(*)0} K^-$ [14]. The invariant mass of two charm hadrons and a beauty baryon were fitted simultaneously, where D^{*0} was partially reconstructed without the π^0/γ contribution. The relative branching fractions were determined as:

$$\frac{\mathcal{B}(\Lambda_b^0 \to \Lambda_c^+ \overline{D}^0 K^-)}{\mathcal{B}(\Lambda_b^0 \to \Lambda_c^+ D_s^-)} = 0.1908^{+0.0036+0.0016}_{-0.0034-0.0018} \pm 0.0038,$$
$$\frac{\mathcal{B}(\Lambda_b^0 \to \Lambda_c^+ \overline{D}^0 K^-)}{\mathcal{B}(\Lambda_b^0 \to \Lambda_c^+ D_s^-)} = 0.589^{+0.018+0.017}_{-0.017-0.018} \pm 0.012,$$

where the first uncertainties are statistical, the second systematic, and the third are due to the uncertainties on the branching fractions of the $D_s^+ \to K^- K^+ \pi^+$ and $\overline{D} \to K^+ \pi^-$.

3. Convention hadron spectroscopy

3.1 Determination of baryon spin parity

Regarding single charm baryons, many of them have been observed by the B factories and the LHCb experiment, but some are not well understand in terms of their excitation nature. Different theories state the explanation on the spin-parity of $\Xi_c(3055)^0$, e.g. hadron molecular state predicting $\frac{1}{2}^-$ or $\frac{3}{2}^-$, while conventional quark model predict D-wave excitation with $\frac{3}{2}^+$ and $\frac{5}{2}^+$, and $2S$ excitation indicating $\frac{1}{2}^+$ and $\frac{3}{2}^+$.

The quantum numbers of $\Xi_c(3055)^{+(0)}$ baryons are determined by an amplitude analysis of $\Xi_b^{0(-)} \to \Xi_c(3055)^{+(0)}(\to D^{+(0)}\Lambda)\pi^-$ [15], which is important to understand the charm baryon spectroscopy. A clear peak can be found in Fig 6.

The significance to reject the spin-parity of $\Xi_c(3055)^+$ and $\Xi_c(3055)^0$ to be $\frac{3}{2}^+$ are 6.5 σ and 3.5 σ, respectively, which favor the prediction of D-wave excitations in terms of charged $\Xi_c(3055)$.

PoS(PIC2024)059

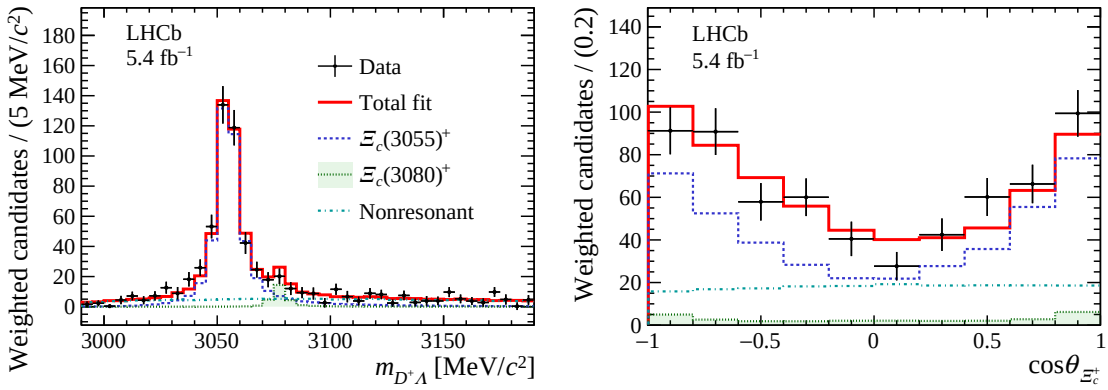

Figure 6: Distributions of the $D^+\Lambda$ invariant mass, Ξ_c^+ helicity angle for the $\Xi_b^0 \to \Xi_c(3055)^+(\to D^+\Lambda)\pi^-$.

3.2 Hidden beauty spectroscopy

While the charmonium system is precisely mapped out, the experimental knowledge of hidden beauty states is more limited. it was shown that the clean experimental signature of χ_c decaying to the $J/\psi\mu^+\mu^-$ final state, referred to as muonic Dalitz decays hereafter, provides a new method to precisely measure properties of charmonia. A similar measurement was also made in the hidden beauty sector at the LHCb experiment. [16] The first observation of the muonic Dalitz decays of the $\chi_{b1}(1P)$, $\chi_{b2}(1P)$, $\chi_{b1}(2P)$ and $\chi_{b2}(2P)$ mesons to the $\Upsilon(1S)\mu^+\mu^-$ system and measurement of the masses of these states is reported as

$$
\begin{aligned}
m_{\chi_{b1}}(1P) &= 9892.50 \pm 0.26 \pm 0.10 \pm 0.10\ \text{MeV}/c^2, \\
m_{\chi_{b2}}(1P) &= 9911.92 \pm 0.29 \pm 0.11 \pm 0.10\ \text{MeV}/c^2, \\
m_{\chi_{b1}}(2P) &= 10253.97 \pm 0.75 \pm 0.22 \pm 0.09\ \text{MeV}/c^2, \\
m_{\chi_{b2}}(2P) &= 10269.67 \pm 0.67 \pm 0.22 \pm 0.09\ \text{MeV}/c^2,
\end{aligned}
$$

where the first uncertainties are statistical, the second systematic and the third are from the limited knowledge of the Υ mass. This paper also report measurement of invariant mass of $\Upsilon(1S)$, $\Upsilon(2S)$ and $\Upsilon(3S)$.

4. Summary and future prospects

In summary, the study of heavy hadron spectroscopy is rapidly advancing, and the data from the LHCb experiment will continue to play a central role in unlocking the mysteries of hadronic physics. As experimental techniques and theoretical models evolve, the next few years hold great promise for further discoveries and a deeper understanding of the strong interaction at the heart of hadronic structure.

References

[1] I. Bezshyiko *et al.* [LHCb], JHEP **11** (2024), 121 doi:10.1007/JHEP11(2024)121 [arXiv:2406.17006 [hep-ex]].

[2] R. Aaij *et al.* [LHCb], Phys. Rev. Lett. **125** (2020), 242001 doi:10.1103/PhysRevLett.125.242001 [arXiv:2009.00025 [hep-ex]].

[3] R. Aaij *et al.* [LHCb], Phys. Rev. D **102** (2020), 112003 doi:10.1103/PhysRevD.102.112003 [arXiv:2009.00026 [hep-ex]].

PoS(PIC2024)059

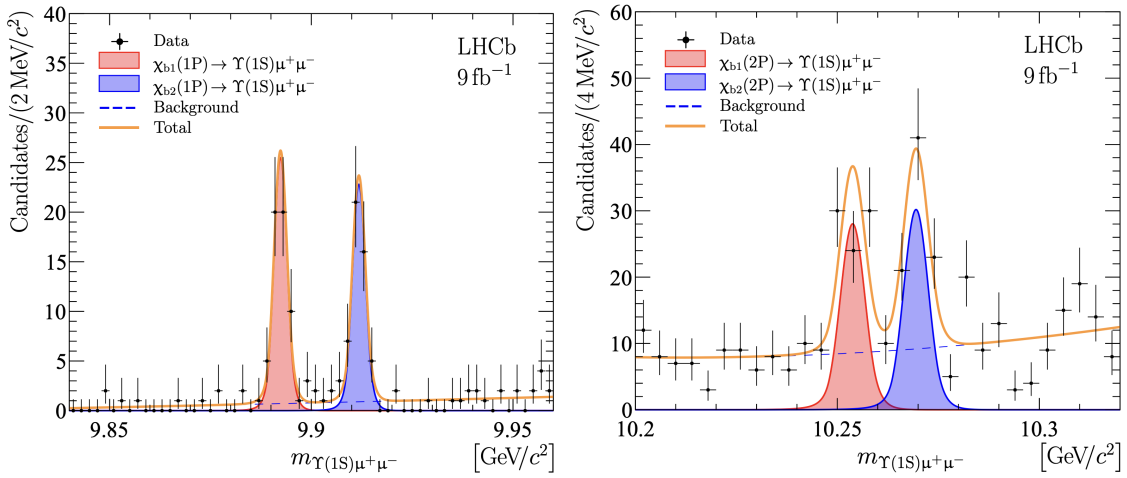

Figure 7: Dimuon mass spectrum. The result of the fit described in the text is overlaid. Mass spectrum of $\Upsilon(1S)\mu^+\mu^-$ candidates in the $\chi_b(1P)$ and $\chi_b(2P)$ region with a constraint on the $\Upsilon(1S)$ mass applied. The result of the fit is overlaid.

[4] R. Aaij *et al.* [LHCb], Phys. Rev. Lett. **131** (2023) no.7, 071901 doi:10.1103/PhysRevLett.131.071901 [arXiv:2210.15153 [hep-ex]].

[5] R. Aaij *et al.* [LHCb], Phys. Rev. Lett. **131** (2023) no.4, 041902 doi:10.1103/PhysRevLett.131.041902 [arXiv:2212.02716 [hep-ex]].

[6] R. Aaij *et al.* [LHCb], Phys. Rev. D **108** (2023) no.1, 012017 doi:10.1103/PhysRevD.108.012017 [arXiv:2212.02717 [hep-ex]].

[7] R. Aaij *et al.* [LHCb], Phys. Rev. Lett. **133** (2024) no.13, 131902 doi:10.1103/PhysRevLett.133.131902 [arXiv:2406.03156 [hep-ex]].

[8] R. Aaij *et al.* [LHCb], JHEP **08** (2024), 165 doi:10.1007/JHEP08(2024)165 [arXiv:2405.00098 [hep-ex]].

[9] R. Aaij *et al.* [LHCb], [arXiv:2411.19781 [hep-ex]].

[10] R. Aaij *et al.* [LHCb], [arXiv:2407.14301 [hep-ex]].

[11] R. Aaij *et al.* [LHCb], Phys. Rev. Lett. **117** (2016) no.8, 082002 doi:10.1103/PhysRevLett.117.082002 [arXiv:1604.05708 [hep-ex]].

[12] R. Aaij *et al.* [LHCb], Phys. Rev. D **110** (2024) no.3, 032001 doi:10.1103/PhysRevD.110.032001 [arXiv:2404.07131 [hep-ex]].

[13] R. Aaij *et al.* [LHCb], Phys. Rev. D **110** (2024) no.3, L031104 doi:10.1103/PhysRevD.110.L031104 [arXiv:2404.19510 [hep-ex]].

[14] R. Aaij *et al.* [LHCb], Eur. Phys. J. C **84** (2024) no.6, 575 doi:10.1140/epjc/s10052-024-12752-3 [arXiv:2311.14088 [hep-ex]].

[15] R. Aaij *et al.* [LHCb], [arXiv:2409.05440 [hep-ex]].

[16] R. Aaij *et al.* [LHCb], doi:10.1007/JHEP10(2024)122 [arXiv:2408.05134 [hep-ex]].

PoS(PIC2024)059